Desalination and Water Treatment
www.deswater.com

doi: 10.5004/dwt.2020.26304

206 (2020) 396–406
December

Performance of a local clay deposit in adsorptive and photochemical removal of Acridine Orange dye and DNA indicator from wastewater

Selma Khelifi[a], Basma Mallah[a], Malika Trabelsi Ayadi[a], Mohamed Habib Oueslati[b], Hassen M. Sbihi[c], Fadhila Ayari[a,*]

[a]*Laboratory of Composite Materials and Clay Minerals, National Center of Researches in Material Sciences, Technopole Borj-Cédria, Tunisia, emails: fadhilaayari@yahoo.fr (F. Ayari), selma.khelifi@gmail.com (S. Khelifi), mellahbesma@yahoo.fr (B. Mellah), malika.trabelsiayadi@gmail.com (M.T. Ayadi)*
[b]*Department of Chemistry, Preparatory Institute for Scientific and Technical Studies, Carthage University, P.O. Box: 51, Marsa 2070, Tunisia, email: oueshabib@yahoo.fr (M.H. Oueslati)*
[c]*Chemistry Department, College of Science, King Saud University, P.O. Box: 2454, Riyadh 1145, Saudi Arabia, email: adam.sbihi@yahoo.com (H.M. Sbihi)*

Received 11 February 2020; Accepted 2 July 2020

ABSTRACT

In this work, adsorptive removal and photocatalytic degradation of Acridine Orange (AO), dye, and DNA indicator has been investigated in aqueous solution using natural clay as adsorbent and photocatalyst in batch mode. The total degradation of AO was tested via UV-vis spectrophotometer and chemical oxygen demand methods. As well, the investigated material was tested in the degradation of a real effluent collected from a Tunisian textile company. Obtained results confirm the high photocatalytic activity of the purified clay for AO mineralization and its great performance in the purification of real wastewater contains organic pollutants. Since the physicochemical characteristic of treated effluent conforms to the norms for reuse in agriculture (NT 106.3 (1989)), this recycling water can be used in irrigation vegetation.

Keywords: Acridine Orange; Natural clay; Adsorption, Photo-Fenton; Degradation; Real wastewater

1. Introduction

Nowadays, water treatment technologies have advanced significantly. However, they still face some molecules that are difficult to degrade, such as pesticides, dyes, and other industrial or agricultural residues. These compounds are called refractory chemical oxygen demand (COD). Large quantities of dyes are used in the textile industry worldwide. This massive use of dyes dangerously threatens water quality and the environment in general [1]. Because of their complexes structure, they are carcinogenic and not biodegradable [2].

Acridine Orange dye (3,6-bis(dimethylamino)Acridine). It is a cationic dye used as fluorescence dyes in molecular biology, toxicology, and supramolecular chemistry [3]. It is often used to probe DNA structure in drug-DNA and protein-DNA interactions [4]. It is difficult to biodegrade due to their complexes aromatic structures. Some researchers were reported in the literature for this dye removal: Jauris et al. [5] studied the efficiency of carbon nanotubes for the adsorptive removal of Acridine Orange dye. Nejad-Darzi et al. [6] interested to the adsorption of Acridine Orange using ZSM-5 nanozeolithe as adsorbent. Zbair et al. [7] evaluated the effectiveness of zinc oxide/almond

* Corresponding author.

shell activated carbon adsorbent for this dye elimination. Also, photochemical removal of Acridine Orange dye was attempted in some works [8,9].

Based on these informations, textile effluents require treatment prior to release. The techniques of oxidation, membrane filtration, ultra, and microfiltration or coagulation by chemical agents can be used for the removal of dyes. These expensive techniques do not definitively eliminate these compounds [10].

In recent decades, advanced oxidation techniques have been one of the most effective ways to achieve total destruction of organic pollutants [11]. Photocatalysis is one of these techniques and has been the subject of many studies; it remains very promising by its ability to destroy organic compounds into simple molecules like CO_2, H_2O, and mineral acids [11,12]. Also, it is based on the high photocatalytic activity of the used catalyst. Then, many authors have been attempted the photodegradation of dye molecules by means of different photocatalysts such as TiO_2 [13], ZnO [3], pillared clay [14], and iron oxide [15].

Adsorption process is a method widely used in the wastewater purification [16]. Referring to the literature, this technique has been used based on activated carbon as adsorbent and the mentioned results show good activity for dye removal [17]. This is due to the simplicity and efficiency of this process. Nevertheless, the high cost of this adsorbent and its difficult regeneration present limits in its application [16]. For these reasons, different alternative adsorbents were developed and applied due to their low cost, abundance, and the possibility of regeneration [18]. Among these adsorbents, natural clays were investigated as inexpensive efficient adsorbents for textile dyes elimination from wastewater such as bentonite [19], sepiolite [20], and pillared clay [18].

So, in this study natural Tunisian clay was prepared and investigated as adsorbent and photocatalyst for Acridine Orange dye removal and real textile effluent treatment.

2. Experimental section

2.1. Reagents and chemicals

2.1.1. Model pollutant

Acridine Orange dye (AO, $C_{17}H_{19}N_3$) is a cationic dye (Fig. 1). It is a dark orange solid and belongs to the family of acridine. Due to their structure, this molecule is used as fluorescence dye in molecular biology toxicology and supramolecular chemistry [3]. AO is selective fluorescent for nucleic acid and it is often used to probe DNA structure in drug-DNA and protein-DNA interactions [4].

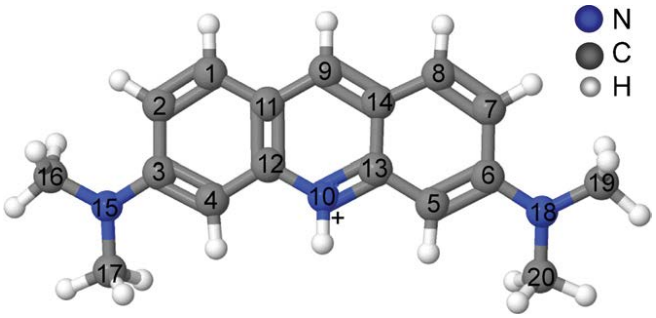

Fig. 1. Chemical structure of Acridine Orange dye.

According to pH value of the dye solution, we defined two forms of AO: AO and AOH^+ and the solution show a sharp change in color [3]. Its molecular weight is 369.94 g mol^{-1}. Its wavelength of maximum absorption in the visible range, determined experimentally, is 585 nm (Fig. 2).

2.1.2. Investigated material

2.1.2.1. Deposit localization

Clay used is natural calcium smectite collected from the deposit of "Kef Abbed" located at north of Tunisia (47 km from Bizerte).

2.1.2.2. Clay purification

Raw clay (RC) was previously crushed and sieved. Hence, 100 g was mixed with 1 L of sodium chloride aqueous solution (1 M) under mechanical agitation for 12 h. After that, obtained suspension was centrifuged for 30 min to collect clay particles. This operation was done many times in order to ensure almost complete substitution of interlayer ions with the sodium ion. Impurities such as quartz and calcite associated with the clay fraction were eliminated by means of sedimentation and centrifugation. Then washed and dialyzed several time [19]. Resulted clay (PC) was dried at 333 K, crushed, and sieved (fraction less than 63 μm was recovered).

2.1.2.3. Clay characterization

Mineralogical analysis were conducted by X-ray diffraction (XRD) using PANalytical X'Pert HighScore Plus diffractometer (Malvern), CuKα radiation (α = 1.5406 Å) source. The range of 2θ is from 2° to 30°. Oriented clay aggregates were prepared by allowing clay-water suspensions to dry at room temperature on three glass slides.

Chemical composition was determined by X-ray fluorescence spectrometer (XRF) using a commercial instrument (ARL 9900 of THERMOFISCER, USA), with monochromatic radiation $K_{\alpha 1}$ of cobalt (λ = 1.788996 Å). Textural properties were carried out via nitrogen adsorption measurements at 77 K with a Quantachrome NOVA 1000^e instrument at 300°C for 3 h. Cation exchange capacity (CEC) was determined by the method of copper ethylenediamine $(EDA)_2CuCl_2$ complex [18]. Thermal analysis was performed by thermogravimetric analysis/differential thermal analysis (TGA/DTA) instrument in the temperature range from 25°C to 1,000°C. Infrared spectra were obtained using Perkin Elmer 783 dispersive spectrometer (Waltham, USA) in the range of 4,000–400 cm^{-1}.

2.2. Experimental section

2.2.1. Adsorption experiments

Examination of dye adsorption onto investigated clay was realized at room temperature (T = 25°C). One-hundred milligrams of clay were added to 50 mL of 10^{-4} mol L^{-1} AO aqueous solution without any further modification of pH

(initial pH = 7). The mixture was agitated for 2 h to reach saturation and then centrifuged at. Residual dye amount measured spectrophotometrically via UV-vis spectrophotometer (Shimadzu Model Perkin Elmer, Kyoto, Japan). The absorbance was monitored at 490 nm. Removal efficiency of the adsorbent was then calculated using Eq. (1):

$$\% \text{ RE} = \frac{C_0 - C_t}{C_0} \times 100 \quad (1)$$

Adsorption capacity (Q_{ads}) was calculated using Eq. (2):

$$Q_{ads} = \frac{\left(C_0 - C_t\right)}{m} V \quad (2)$$

where C_0 is the initial dye concentration, C_t is the dye concentration at t, m is the mass of the adsorbent used (g), and V is the volume of dye solution (L).

2.2.2. Advanced oxidation process experiments

Photo-Fenton experiments were carried out at room temperature (T = 25°C) in a cylindrical photoreactor under UV light irradiation (λ = 350°C). Acridine Orange dye was oxidized by H_2O_2 using purified clay as photo-Fenton heterogeneous catalyst. The initial concentration of CR was 10^{-4} mol L^{-1} and the total volume of the reaction solution was 150 mL. First of all, 100 mg of adsorbent was mixed with 150 mL of dye solution stirred for 60 min, the suspension was putted under UV irradiation and at specific time, 3 mL of solution were extracted and centrifuged to separate the photocatalyst from dye solution. Concentration of AO at a different solution was quantified by measuring the absorbance at 585 nm.

3. Results and discussion

3.1. Adsorbent characterization

3.1.1. Chemical composition and structural formula determination

Chemical compositions of RC and PC were reported in Table 1. Loss on ignition values of raw and purified clay are 22.5% and 20.31%, respectively.

According to these mentioned results and refereeing to some reviews [19,23], we noted the following remarks:

- The ration $\frac{SiO_2}{\left(Al_2O_3 + MgO + Fe_2O_3\right)}$ is close to 2 which indicates that studied clay is of 2:1 type.
- Amount of K_2O increased after purification, this is due to the existence of illite fraction in the clay sample.

The chemical formula of purified clay PC was determined according to the method developed by Mauguin [21], which consists of transforming the weight proportions obtained by the chemical analysis into a number of the atom–gram of oxygen and then decomposing each oxide into the number of oxygen and cation. The calculations are reduced to 22 atoms of oxygen (number of oxygen per mesh of calcined clay of 2:1 type).

3.1.1.1. Charge deficit in the tetrahedral layer

In the PC sample, the Si atom number = 7.87.

The charge deficit in the tetrahedral layer is then: 8 – 7.87 = 0.13.

This deficit = 0.13 corresponds to an equivalent number of Al^{3+} cation of the octahedral layer.

3.1.1.2. Charge deficit in the octahedral layer

$$(n(Al^{3+}) + n(Fe^{3+}) - 0.44) \times 3 + n(Mg^{2+}) \times 2 = 11.32$$

Hence the charge deficit in the octahedral layer: 12 – 11.32 = 0.671.

3.1.1.3. Sum of the deficits of charges

Total charge deficit: 0.671 + 0.13 = 0.801

The sum of charges of interfoliar cations (K^+, Na^+, and Ca^+) is 0.674.

So according to these calculations, the structural formula is presented as follow:

$$Ca_{0.05}Na_{0.145}K_{0.479}(Si_{7.87}Al_{0.13})(Al_{2.6}Fe_{0.678}Mg_{0.547})O_{22}$$

The number of atoms in the octahedral layer approaches to 4 which confirms the dioctaedric character already deduced by calculating the SiO_2 ratio by (Al_2O_3 + MgO + Fe_2O_3).

3.1.2. XRD analysis

X-ray diffraction analysis was conducted to investigate the structure of raw and purified clays. XRD patterns of both samples are presented in Fig. 3. According to these results, it can be concluded that:

- Initial peak at 15.3 Å which moves toward 12.38 Å after purification proving that the clay sample used is a smectite, naturally calcium, which has become sodic after purification.
- Two peaks at 4.27 and 3.35 Å defined the presence of quartz which is disappeared after purification.
- Peaks at 7.11 and 3.57 Å suggested the presence of kaolinite fraction associated with the studied clay sample [22].
- Presence of illite fraction was confirmed by a peak at 10.32 Å inspiring the existence of a portion of illite associated with the smectitic fraction.

Diffractograms of oriented samples are presented in Fig. 4. According to these results, it can be noted that the smectitic nature is indicated by the existence of peaks at 17.69 Å after ethylene glycol treatment. The kaolinite fraction was confirmed by the existence of peaks at 7.19 and 3.57 Å on the glycoled diffractograms which disappear after calcinations at 550°C during 2 h.

Results indicate that this clay has a swelling character, belonging to the smectite family which is associated with kaolinite and illite fractions.

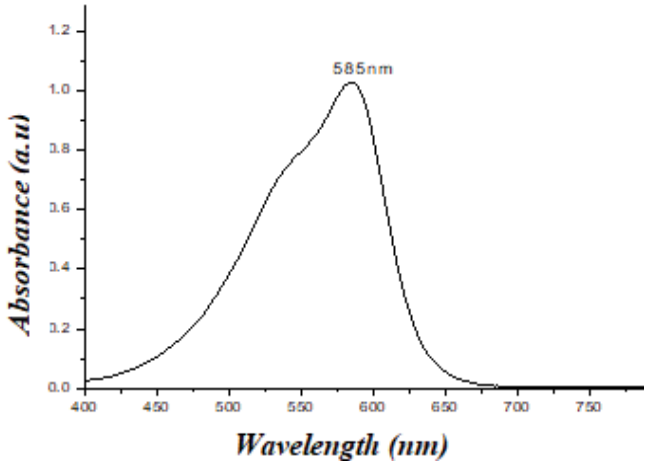

Fig. 2. UV-Visible spectra of Acridine Orange dye.

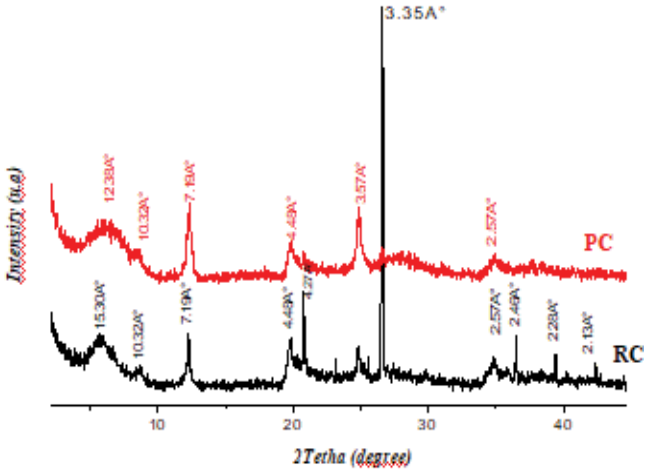

Fig. 3. XRD patterns of raw (RC) and purified (PC) clays.

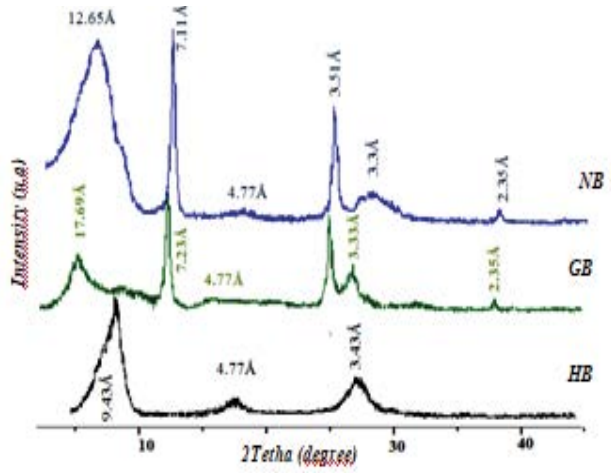

Fig. 4. Diffractograms of oriented samples of purified clay (PC) (HB: heated blade; GB glycol blade; NB: normal blade).

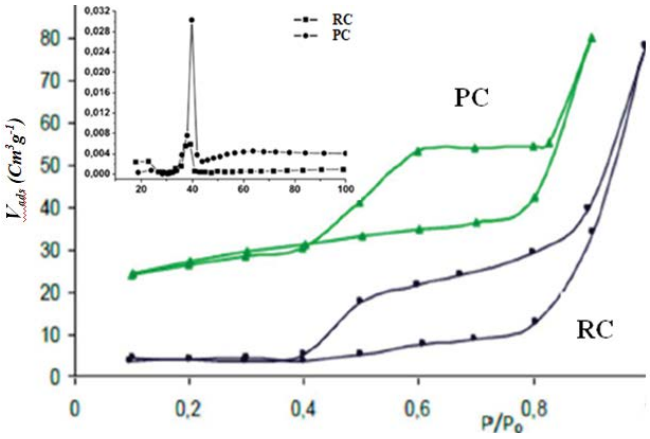

Fig. 5. BET surface area calculated from nitrogen adsorption–desorption isotherms for both clay samples. The insets present the pore size distribution.

3.1.3. Textural and structural properties

Porosity of clay samples was probed by N_2 adsorption–desorption studies. Fig. 5 shows the isotherm curves of both samples with the pore size distribution calculated using the Barrett–Joyner–Halenda (BJH) method (inset of Fig. 5). Purified clay PC presents the high surface area 72.2 m^2 g^{-1}, the surface area of the raw clay RC was 35 m^2 g^{-1} (Table 3). The increase in the surface is related to the impurities elimination after purification process. Brunauer–Emmett–Teller (BET) surface area, pore volume, and average pore diameter of both samples are presented in Table 2. Also, CEC measurement was performed and obtained results (Table 2) show the increase of CEC after purification.

Table 1
Chemical composition of raw (RC) and purified clay (PC)

Oxides (wt.%)	RC	PC
SiO_2	40.66	52
MgO	3.53	4.2
CaO	19	4.0
Fe_2O_3	4.89	4.8
Al_2O_3	9.23	15.3
Na_2O	1.16	1.63
K_2O	0.43	0.76
*LOI	22.5	20.31

*LOI: Loss on ignition.

3.1.4. Infrared analysis

The FTIR spectra of purified and raw sample are shown in Fig. 6. The broad band's at around 3,419 cm^{-1} (H–O–H stretching) and 1,646 cm^{-1} (H–O–H bending) indicate the presence of adsorbed water. The presence of an asymmetric stretching mode of Si–O–Si was suggested by the absorption bands at the range of 1,035–1,123 cm^{-1}. The asymmetric and symmetric bending modes of O–Si–O are observed at 536 and 469 cm^{-1}, as in other silica and silicate systems.

The additional peaks at 686 and 796 cm^{-1} in raw clay, which are absent in purified clay (PC), indicate the presence

Table 2
Most important properties of used samples RC and PC

	S_{BET} ($m^2\ g^{-1}$)	V_{ads} ($Cm^3\ g^{-1}$)	D (Å)	CEC (méq/100 g)
Raw (RC)	35	0.06	19.003	60.52
Purified (PC)	72.2	0.07	19.1	110.76
Structural formula: $Ca_{0.05}Na_{0.145}K_{0.479}(Si_{7.87}Al_{0.13})\ (Al_{2.6}Fe_{0.678}\ Mg_{0.547})O_{22}$				

of quartz accompanying the raw sample, eliminated after purification [23].

3.1.5. Optical properties

UV-visible diffuse reflectance spectra of clay samples before and after purification (Fig. 7) shows that the raw clay exhibited one edge absorption in the ultraviolet region at 240 nm. After purification, the purified clay exhibited an additional band edge in the visible light region at 600 nm. This result indicated that optical response of purified clay PC could be extended to the visible light field. According to Tanwar et al. [24], this visible light energy can be used by the material for realizing the photocatalytic activity.

3.2. Treatment of dye aqueous solution

3.2.1. Adsorption study

3.2.1.1. Kinetics of adsorption

Adsorption data of AO dye onto RC and PC samples versus contact time are presented in Fig. 8. According to this figure, adsorption kinetics of AO by purified clay (PC) and raw clay (RC) takes the same forms characterized by a quick increase of the percentage adsorption in the first minutes of contact time (adsorbate – adsorbent), followed by a slow increase until reaching equilibrium which is less than 30 min. The highest percent of AO removal was attributed to purified clay PC sample (Fig. 8).

3.2.1.2. Effect of initial pH value

Adsorption efficiency of AO onto purified clay versus initial pH (2–10) is presented in Fig. 9. Adsorbed amount of AO dye increase with the increase of pH from 2 to 6. At the higher value of pH, the adsorbed amount decrease which is explained by the interaction between dye protons AOH^+ and OH^- ions in the solution.

3.2.1.3. Effect of temperature

Adsorption of AO onto purified clay at 303, 313, and 323 K (Fig. 10) indicated that adsorption percent decreased with increase of temperature from 303 to 323 K, indicating the exothermic nature of the adsorption process.

3.2.1.4. Adsorption isotherms

Adsorption isotherms are of *S* type (Fig. 11) suggested adsorbent affinity to the adsorbed substrate [25].

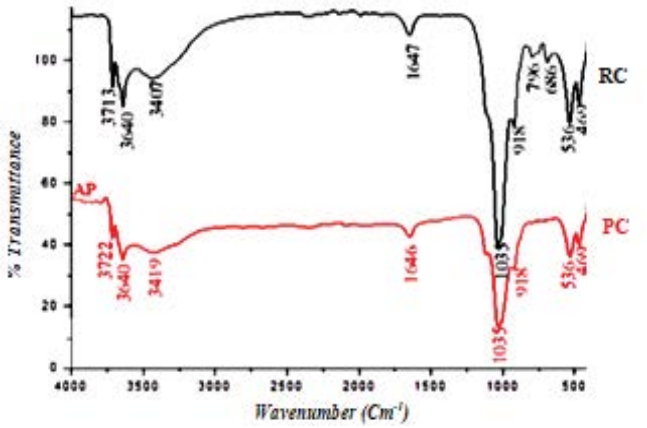

Fig. 6. Infrared spectra of studied clay before and after purification.

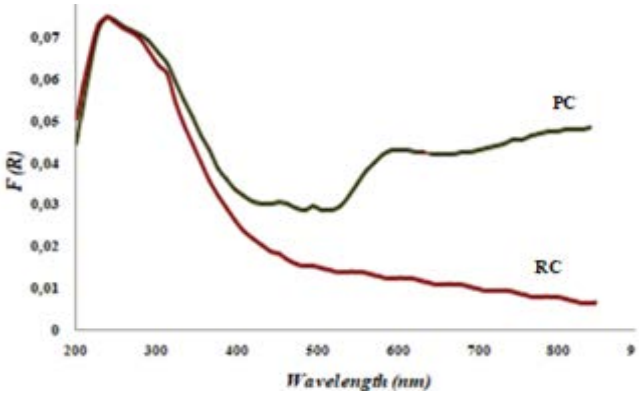

Fig. 7. Optical absorbance spectra of both clay samples.

The rate of dye adsorption onto RC, containing impurities, is obviously lower then that obtained by PC (Q_{ads} (PC = 1.6 × Q_{ads} (RC)). Impurities inhibit the adsorption.

3.2.2. Analysis of data using various adsorption models

To better understand the mechanism of adsorption of AO by purified clay, it is necessary to modeling the experimental results. Adsorption data of AO by purified clay were analyzed according to Langmuir and Freundlich isotherm models.

3.2.2.1. Langmuir model

Langmuir isotherm was defined to describe monolayer sorption process. Linear equation of this model is presented as follows [26]:

$$\frac{C_e}{q_e} = \frac{1}{Q_0} + \left(\frac{b}{Q_0}\right) C_e \quad (3)$$

where C_e (g L^{-1}) is the residual amount of AO at equilibrium, q_e (g g^{-1}) is the amount of dye adsorbed, Q_0 and b are the Langmuir constant related to adsorption capacity and rate of adsorption, respectively.

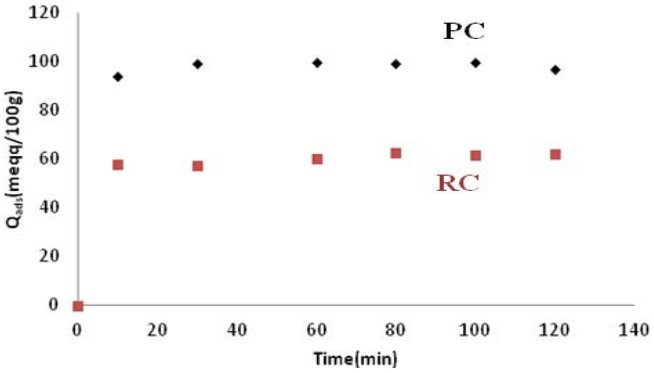

Fig. 8. Adsorption kinetics of AO dye onto the raw RC and purified PC clays.

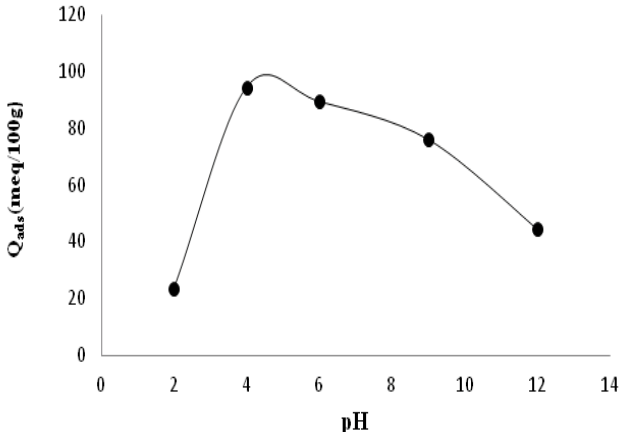

Fig. 9. Effect of pH on adsorption of AO onto purified clay.

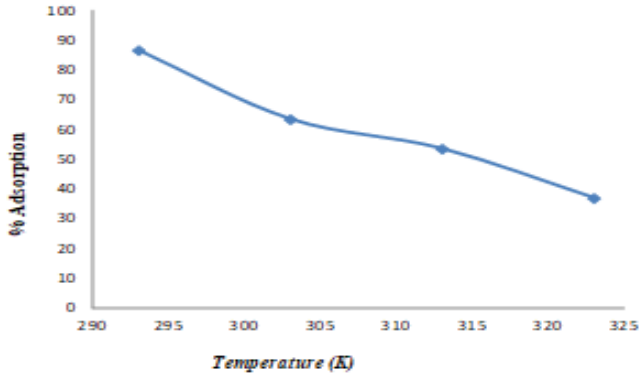

Fig. 10. Effect of temperature on adsorption of AO onto purified clay (PC).

Results (Fig. 12, Table 3) show that experimental data fit very well with the Langmuir model (R^2 = 0.96), suggested a monolayer adsorption process. Langmuir parameters, b and Q_0, were mentioned in Table 3.

3.2.2.2. Freundlich model

Freundlich model is often used to describe non-specific adsorption. Linear form of the equation is presented as follow [27]:

$$\log q_e = \log K_F + \frac{1}{n}\log C_e \quad (4)$$

where q_e is the adsorbed amount (g/g), C_e is the equilibrium concentration. K_F and n are Freundlich parameters, n specified if the adsorption process is favorable, K_F (g/g (L/g)$^{1/n}$) sorption capacity.

$1/n \in [0,1]$, gives information about the surface heterogeneity [19,23].

Freundlich model is not suitable to describe AO sorption by PC (Fig. 13, Table 3). Freundlich parameters (K_F and n) were mentioned in Table 4.

3.2.2.3. Mechanism adsorption kinetics

Infrared spectroscopy confirms the adsorption of AO (Figs. 13a and b) by the purified clay sample. Indeed, by comparing the IR spectrum of the purified clay before

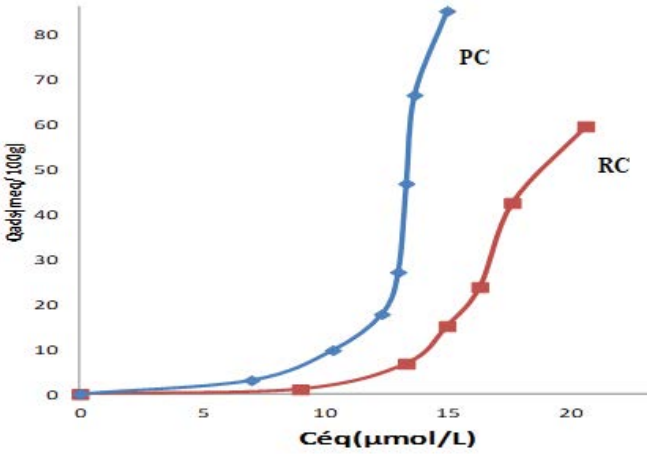

Fig. 11. Effect of initial dye concentration of AO on the raw and purified clay.

Table 3
Langmuir and Freundlich parameters of AO adsorption by PC

Isotherm	Parameter
Langmuir	Q_0 = 0.00243
	b = –0.068
Freundlich	$K_F = 1.5 \times 10^{-8}$
	n = –0.29

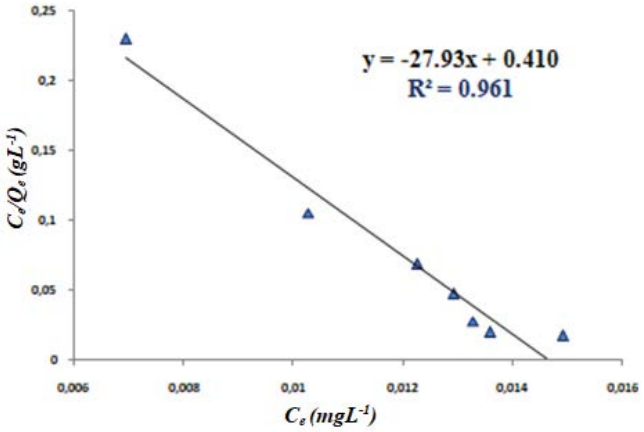

Fig. 12. Langmuir isotherm of AO adsorption by PC.

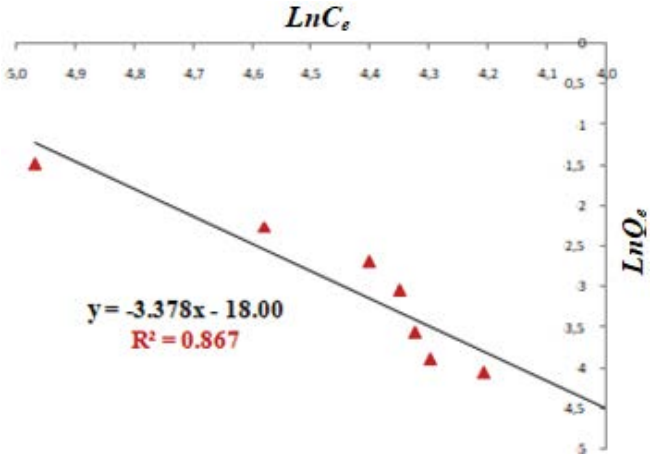

Fig. 13. Freundlich isotherm of AO adsorption onto PC.

and after adsorption of the AO dye and referring to the IR spectrum of the latter (Fig. 14c), we have to note the appearance of certain characteristic bands of this complex: purified clay saturated with AO dye (Table 4). These results suggest that AO intercalates well the clay network.

The infrared spectra reveal that the intensity of the absorption bands is a function of the dye concentration; it increases proportionally with the latter. This is in perfect agreement with the literature [17,28].

3.2.3. Oxidation study

After Fenton oxidation (Fig. 15a), photocatalytic activity of the studied samples under same conditions was studied as that for the dark system.

Fig. 15b presents the optical absorbance of AO as a function of irradiation time using clay as catalysts under UV irradiation. As can be seen in this figure, the removal efficiency of AO increase quickly and completely within 60 min in the presence of purified clay PC photocatalyst and reached 80% of degradation percent which is four times greater than the raw clay RC (20% removal efficiency after 3 h). The short photodegradation time and the high removal efficiency of AO in the presence of PC sample might be due to its high energy of UV compared with RC sample. Also, this is well confirmed by photoluminescence analysis.

Fig. 16 shows PL spectra of raw and purified clays done at an excitation wavelength of 400 nm. As can be seen, the raw clay RC and its purified fraction exhibit similar emission trends, with the principal peak around 535 nm. The raw clay RC was found to have a higher PL intensity than the PC. This indicates that RC had the highest optical recombination rate, which may deteriorate the photodegradation efficiency compared with the purified clay PC which had a lower rate of recombination of photoelectrons. Hence, these results confirm that the purified clay PC presents a good photocatalytic activity compared with that of the raw clay RC. In their previous study [29] confirm that material with lower PL intensity, has less recombination of photo-induced electron-hole pairs which is results of an enhancement in photocatalytic activity.

3.2.3.1. Photocatalytic degradation of AO under UV irradiations by different ways

The photochemical treatment of AO dye by different ways were presented as follow: $C_{(t)}/C_0$ as a function of the irradiation time (C_0 is the concentration before irradiation, and $C_{(t)}$ is the dye concentration; Fig. 17).

It is seen that 85% of the initial concentration of the dye was removed after 120 min irradiation and 69% of COD removal was observed with 120 min irradiation time (Table 5) by photo-Fenton process using purified clay PC as catalyst. In contrast, a negligible decrease in the concentration of the dye was observed by irradiation in the absence of H_2O_2 (10% of dye removal) or in the presence UV irradiation without catalyst (Fig. 17, Table 5). Under UV light irradiation in the presence of hydrogen peroxide, AO degradation is important (67% of dye removal) because of the reaction between hydrogen peroxide and UV light to produce hydroxyl radicals [30].

3.2.3.2. Stability of the studied photocatalyst

Stability of catalyst is an important characteristic in this field. For this reason, stability of purified clay PC under UV light irradiation was evaluated. The photocatalytic performance was measured in three cycles (Fig. 18). Under these operating conditions: $[AO]_0 = 10^{-4}$ mol L^{-1}, $[H_2O_2]_0 = 10$ mmol L^{-1}, $pH_0 = 7$, and $T = 25°C$.

It is clearly seen that PC photocatalyst indicates a negligible change in photo-oxidation performance; also we note a

Table 4
Principal bands in infrared spectrum of purified clay (PC) after AO dye adsorption

Attribution	Corresponding bands
$\delta(C_{ar}–H)$	650–800
$\upsilon(C=C)_{ar}$	1,592
$\upsilon(C=NH^+)$	2,000–2,300
$\upsilon(C_{ar}–N)$	1,363

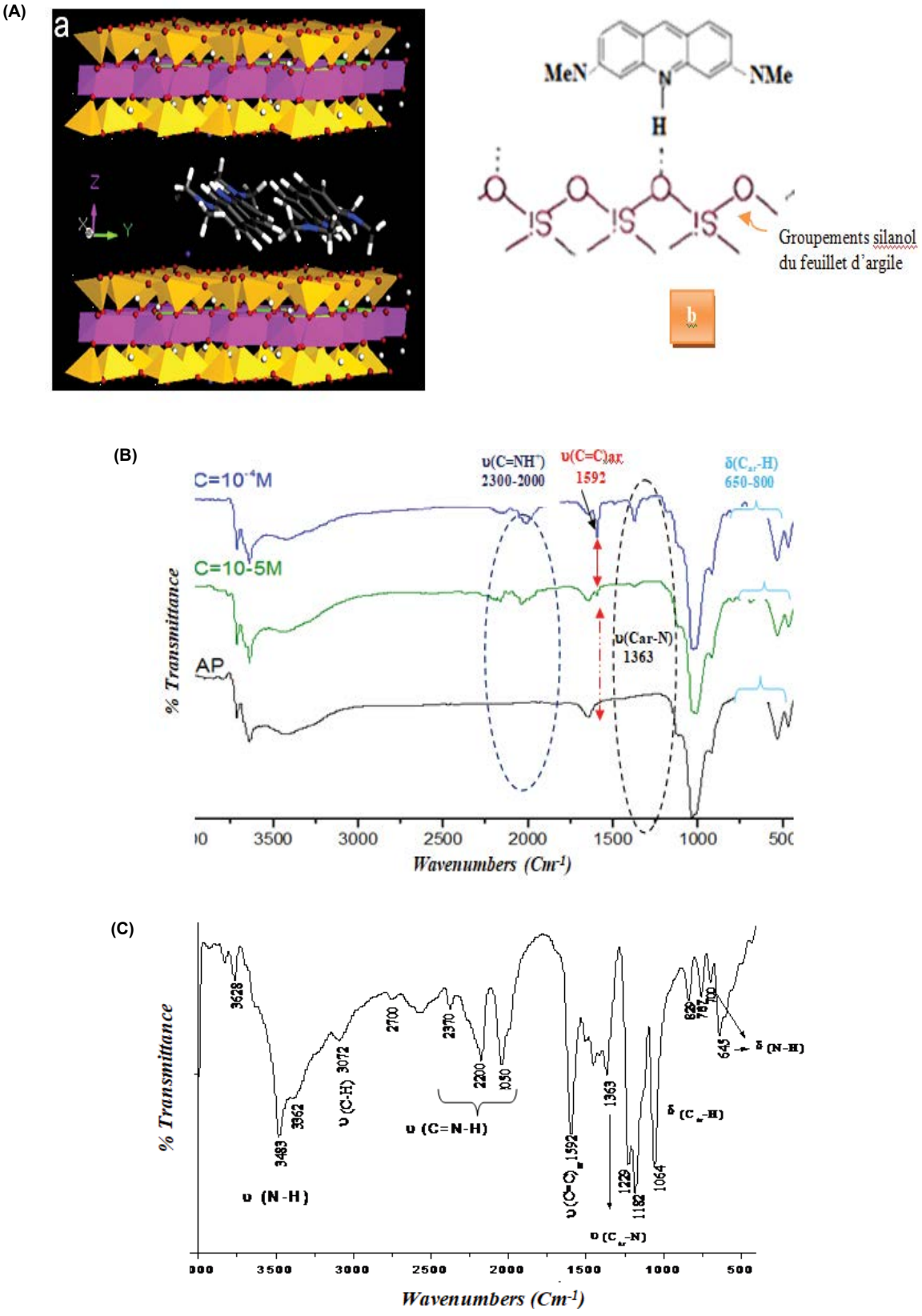

Fig. 14. (A) Adsorption of Acridine Orange dye by the purified clay. Infrared spectrum of (B) purified clay before and after AO dye intercalation (with two different concentrations) and (C) Acridine Orange dye.

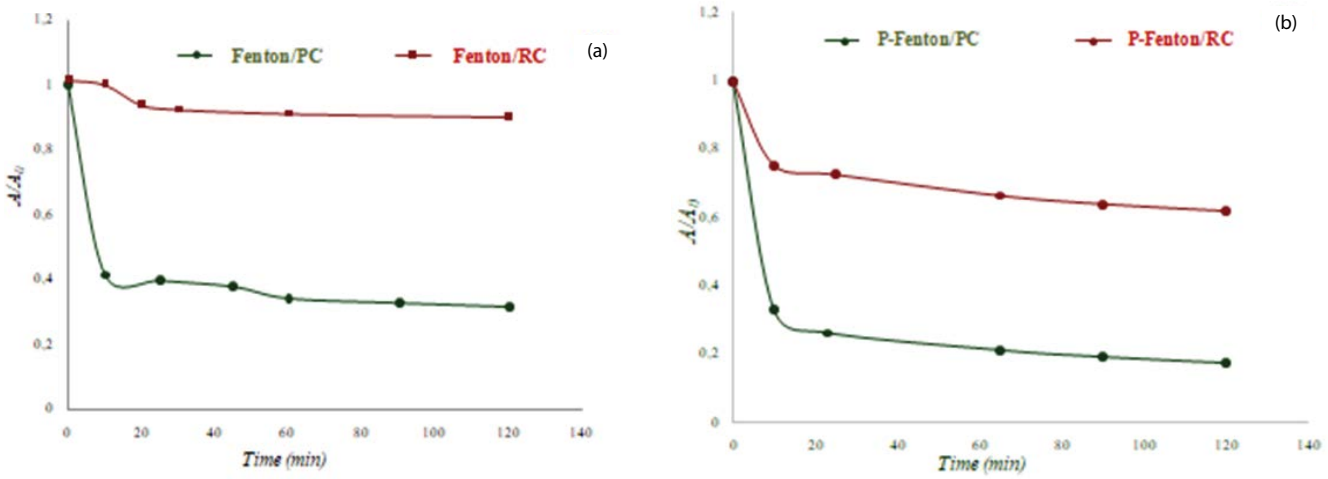

Fig. 15. Relative optical absorbance for AO degradation by (a) Fenton and (b) photo-Fenton processes in the presence of raw and purified clays.

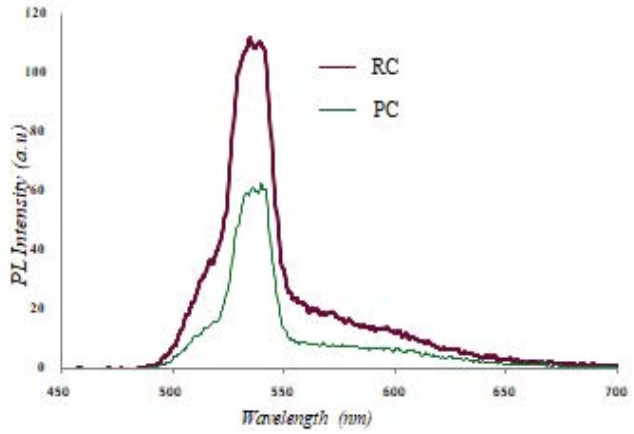

Fig. 16. Photoluminescence spectra for raw and purified clays (Excitation wavelength = 400 nm).

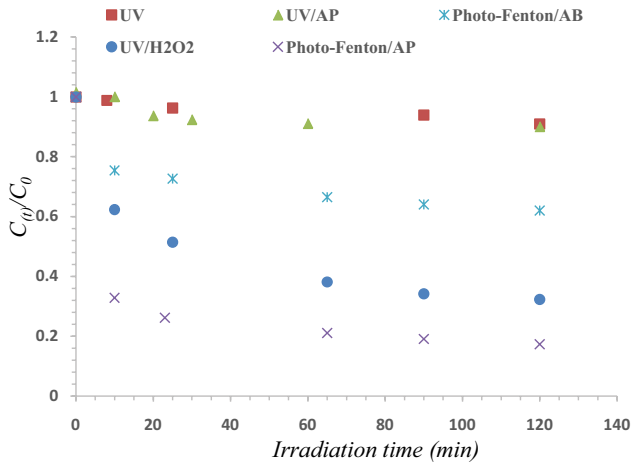

Fig. 17. Relative concentration $C_{(t)}/C_0$ for AO photodegradation by different ways.

low decrease in activity at the third time compared with the first time.

These results confirm that the purified clay PC has a high stability which can be investigated as material in wastewater treatment.

3.2.3.3. Photocatalytic degradation of a real textile wastewater

Obtained results of Acridine Orange dye treatment using purified clay as adsorbent and photocatalyst confirm the high catalytic activity of this natural material for dye removal. These results let us think to test this process in the degradation of a real effluent. For this reason, a sample of wastewater was collected from a Tunisian textile company (SARTEX). Table 6 presents the characteristics of the studied effluent before and after treatment.

Experiment was carried out as follows: desired amount of purified clay PC (1 g) was shaken in the dark with 150 mL of real effluent at room temperature for the establishment of the adsorption equilibrium. Then, hydrogen peroxide H_2O_2 was added to the reaction medium and the lamp was turn off. As can be seen in Table 6, physicochemical parameters of studied effluent decrease compared to them before treatment. pH reaches a low value; for this reason, treated effluent can be released in aquatic medium (6 < pH < 8.5) [31]. Also, for the COD measurement we

Table 5
Degradation percent of AO and chemical oxygen demand (COD) analysis of dye solution in all cases

Sample details	% Degradation	% DCO
UV	7%	0.4%
UV/H_2O_2	67%	30%
UV/PC	10%	2%
UV/H_2O_2/PC	85%	69%
UV/H_2O_2/RC	25%	15%

Table 6
Most characteristics of real wastewater before treatment

Quality indicators	Values before treatment	Values after treatment
pH	10	8
TOC	10	1.6
DBO_5	600	90
COD	1,400	600
TDS	3,500	2,400
Chlorides	1,700	700
Oil and grease	10	0.04
Total hardness	100	0.3
Suspended solids	200	2
Color	3,500	1,050

Table 7
Comparison of catalytic activity for different catalysts

Catalyst	Pollutant	% degradation	Reference
ZnO modified bentonite	Methylene blue	87	[33]
Natural purified clay	Acridine Orange dye	88	This work
Zinc Oxide	Acridine Orange dye	90	[3]
ZnO modified bentonite	phenol	90	[33]
Clay mineral/CdS	Congo Red dye	93	[34]

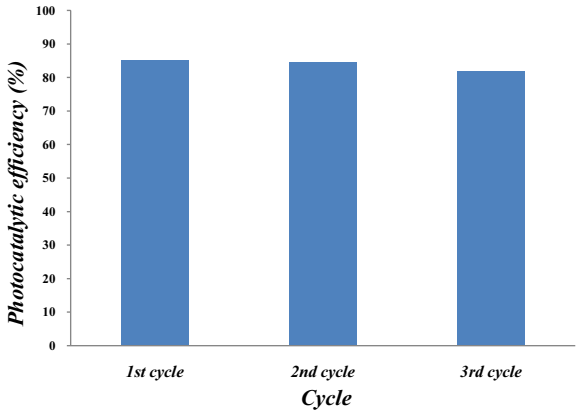

Fig. 18. Cycling test of AP catalyst up to three times under UV illumination towards AO.

note a 50 % of COD removal, which allow the discharge in public sewage systems and in aquatic medium. Also, the color removal was achieved 70% which is considered an efficient result. According to these results, the treated water quality obeys the norms for reuse in agriculture [32] which can be used for vegetation adapted to high salinity.

In this section, a comparative study between this work and others was established regarding the application of different photocatalyst in photo-Fenton degradation of organic pollutants. For this purpose, Table 7 illustrates the results obtained in terms of degradation efficiency in the presence of natural clay investigated in this study and other catalysts mentioned in published works.

According to these results, we can conclude the efficiency and the good activity of the investigated material which specify the importance of this work in the research.

4. Conclusion

Clay used is an effective and good adsorbent for Acridine Orange dye elimination from wastewater because of high adsorptive capacity and the short adsorption time without any modification of pH before treatment. Adsorptive removal of AO dye by smectite clay was a spontaneous and exothermic process. The uptake of AO onto the used clay was studied by evaluation of different parameters: contact time, initial dye concentration, pH, and temperature. Good agreement with the Langmuir model being denoted confirmed by a correlation coefficient of R^2 = 0.96. The photo-Fenton process can be applied to remove the Acridine Orange dye using natural purified clay as photocatalyst. So, according to obtained results in this study, it can be concluded that the studied clay has a high catalytic activity under UV irradiations light. Also, Stability experiments showed that purified clay was stable and can be used for several tests without loss in catalytic activity or chemical structure.

Finally, the photo-Fenton system using purified clay is a promising process for dye mineralization and the treatment of real effluent from textile industries.

Acknowledgments

The authors would like to extend their sincere appreciation to King Saud University (Riyadh, Saudi Arabia) for

the support of this research through Researchers Supporting Project number (RSP-2020/137).

References

[1] C. Galindo, P. Jacques, A. Kalt, Photochemical and photocatalytic degradation of an indigo dye: a case study of acid blue 74(AB74), J. Photochem. Photobiol., A, 141 (2001) 47–56.

[2] H. Hou, R. Zhou, P. Wu, L. Wu, Removal of Congo red dye from aqueous solution with hydroxyapatite/chitosan composite, Chem. Eng. J., 211 (2012) 336–342.

[3] B. Pare, S.B. Jonnalagadda, H. Tomar, P. Singh, V.W. Bhagwat, ZnO assisted photocatalytic degradation of acridine orange in aqueous solution using visible irradiation, Desalination, 232 (2008) 80–90.

[4] C.C. Chen, R.J. Wu, Y.Y. Tzeng, C.S. Lu, Chemical oxidative degradation of acridine orange dye in aqueous solution by Fenton's reagent, J. Chin. Chem. Soc., 56 (2009) 1147–1155.

[5] I.M. Jauris, S.B. Fagan, M.A. Adebayo, F.M. Machado, Adsorption of acridine orange and methylene blue synthetic dyes and anthracene on single wall carbon nanotubes: a first principle approach, Comput. Theor. Chem., 1076 (2016) 42–50.

[6] S.K.H. Nejad-Darzi, A. Samadi-Maybodi, M. Ghobakhluo, Synthesis and characterization of modified ZSM-5 nanozeolite and their applications in adsorption of Acridine orange dye from aqueous solution, J. Porous Mater., 20 (2013) 909–916.

[7] M. Zbair, Z. Anfar, H.A. Ahsaine, N. El Alem, M. Ezahri, Acridine orange adsorption by zinc oxide/almond shell activated carbon composite: operational factors, mechanism and performance optimization using central composite design and surface modeling, J. Environ. Manage., 206 (2018) 383–397.

[8] R. Selvaggi, L. Tarpani, A. Santuari, S. Giovagnoli, L. Latterini, Silica nanoparticles assisted photodegradation of acridine orange in aqueous suspensions, Appl. Catal., B, 168 (2015) 363–369.

[9] I. Ahmad, S.B. Khan, T. Kamal, A.M. Asiri, Visible light activated degradation of organic pollutants using zinc–iron selenide, J. Mol. Liq., 229 (2017) 429–435.

[10] M. Tekbaş, H.C. Yatmaz, N. Bektaş, Heterogeneous photo-Fenton oxidation of reactive azo dye solutions using iron exchanged zeolite as a catalyst, Microporous Mesoporous Mater., 115 (2008) 594–602.

[11] H. Lin, H. Zhang, X. Wang, L. Wang, J. Wu, Electro-Fenton removal of Orange II in a divided cell: reaction mechanism, degradation pathway and toxicity evolution, Sep. Purif. Technol., 122 (2014) 533–540.

[12] S. Khelifi, F. Ayari, A. Choukchou-Braham, D. Ben Hassen Chehimi, The remarkable effect of Al-Fe pillaring on the adsorption and catalytic activity of natural Tunisian bentonite in the degradation of azo dye, J. Porous Mater., 25 (2018) 885–896.

[13] H. Chaker, L. Chérif-Aouali, S. Khaoulani, A. Bengueddach, S. Fourmentin, Photocatalytic degradation of methyl orange and real wastewater by silver doped mesoporous TiO_2 catalysts, J. Photochem. Photobiol., A, 318 (2016) 142–149.

[14] S. Khelifi, F. Ayari, Modified bentonite for anionic dye removal from aqueous solutions. Adsorbent regeneration by the photo-Fenton process, C. R. Chim., 22 (2019)154–160.

[15] F. Ayari, A.B. Othmen, S. Khelifi, M. Trabelsi-Ayadi, Photodegradation of Congo red and real textile industries effluent using natural Tunisian iron oxide, Desal. Water Treat., 107 (2018) 316–323.

[16] C. Srilakshmi, R. Saraf, Ag-doped hydroxyapatite as efficient adsorbent for removal of Congo red dye from aqueous solution: synthesis, kinetic and equilibrium adsorption isotherm analysis, Microporous Mesoporous Mater., 219 (2016) 134–144.

[17] A. Berez, G. Schäfer, F. Ayari, M. Trabelsi-Ayadi, Adsorptive removal of azo dyes from aqueous solutions by natural bentonite under static and dynamic flow conditions, Int. J. Environ. Sci. Technol., 13 (2016) 1625–1640.

[18] J.L. Marco-Brown, C.M. Barbosa-Lema, R.M.T. Sánchez, R.C. Mercader, M. Afonso, Adsorption of picloram herbicide on iron oxide pillared montmorillonite, Appl. Clay Sci., 58 (2012) 25–33.

[19] F. Ayari, E. Srasra, M. Trabelsi-Ayadi, Characterization of bentonitic clays and their use as adsorbent, Desalination, 185 (2005) 391–397.

[20] Z. Wang, L. Liao, A. Hursthouse, N. Song, B. Ren, Sepiolite-based adsorbents for the removal of potentially toxic elements from water: a strategic review for the case of environmental contamination in Hunan, China. Int. J. Environ. Res. Public Health, 15 (2018) 1653, doi: 10.3390/ijerph15081653.

[21] C. Mauguin, Etude Des Micas au Moyen des RX Bull, Soc. Fr. Miner., 269 (1928) 815–818.

[22] G. Brown, G.W. Brindley (Eds.), Crystal Structures of Clay Minerals and Their X-Ray Identification, Vol. 5, Mineralogical Society, London, 1980, pp. 305–360.

[23] F. Ayari, E. Srasra, M. Trabelsi-Ayadi, Retention of lead from an aqueous solution by use of bentonite as adsorbent for reducing leaching from industrial effluents, Desalination, 206 (2007) 270–278.

[24] R. Tanwar, S. Kumar, U.K. Mandal, Photocatalytic activity of PANI/Fe^0 doped BiOCl under visible light-degradation of Congo red dye, J. Photochem. Photobiol., A, 333 (2017) 105–116.

[25] C.H. Giles, T.H. MacEwan, S.N. Nakhwa, D. Smith, Studies in adsorption. Part XI. A system of classification of solution adsorption isotherms, and its use in diagnosis of adsorption mechanisms and in measurement of specific surface areas of solids, J. Chem. Soc., 786(1960) 3973–3993.

[26] I. Langmuir, The adsorption of gases on plane surfaces of glass, mica and platinum, J. Am. Chem. Soc., 40 (1918) 1361–1403.

[27] H.M.F. Freundlich, Uber die adsorption in losungen, zeitschrift fur phtsikalische chemie, Am. Chem. Soc., 62 (1906) 121–125.

[28] F. Ayari, M.T. Ayadi, Inorganic and organic smectite for synthetic and real textile water treatment, optical and luminescence properties, Desal. Water Treat., 125 (2018) 47–60.

[29] P. Li, C. Liu, G. Wu, Y. Heng, S. Lin, A. Ren, W. Shi, Solvothermal synthesis and visible light-driven photocatalytic degradation for tetracycline of Fe-doped $SrTiO_3$, RSC Adv., 4 (2014) 47615–47624.

[30] O. Krik, Encyclopedia of Chemical Technology, 4th ed., John Wiley & Sons, New York, NY, 1993, p. 753.

[31] NT 106.02 TS-BoJbtMotNE, Implementing the Tunisian Standard Concerning Wastewater Effluent Discharges in the Hydrous Medium, 1989.

[32] NT 106.03 TS-DoDMtDoJbtMotNE, Implementing the Tunisian Standard Concerning the Use of Treated Wastewater in Agriculture, 1989.

[33] S.P. Sasikala, T.A. Nibila, K.B. Babitha, A.A.P. Mohamed, A. Solaiappan, Competitive photo-degradation performance of ZnO modified bentonite clay in water containing both organic and inorganic contaminants, Sustainable Environ. Res., 29 (2019) 1.

[34] X. Wang, B. Mu, A. Hui, A. Wang, Comparative study on photocatalytic degradation of Congo red using different clay mineral/CdS nanocomposites, J. Mater. Sci. - Mater. Electron., 30 (2019) 5383–5392.